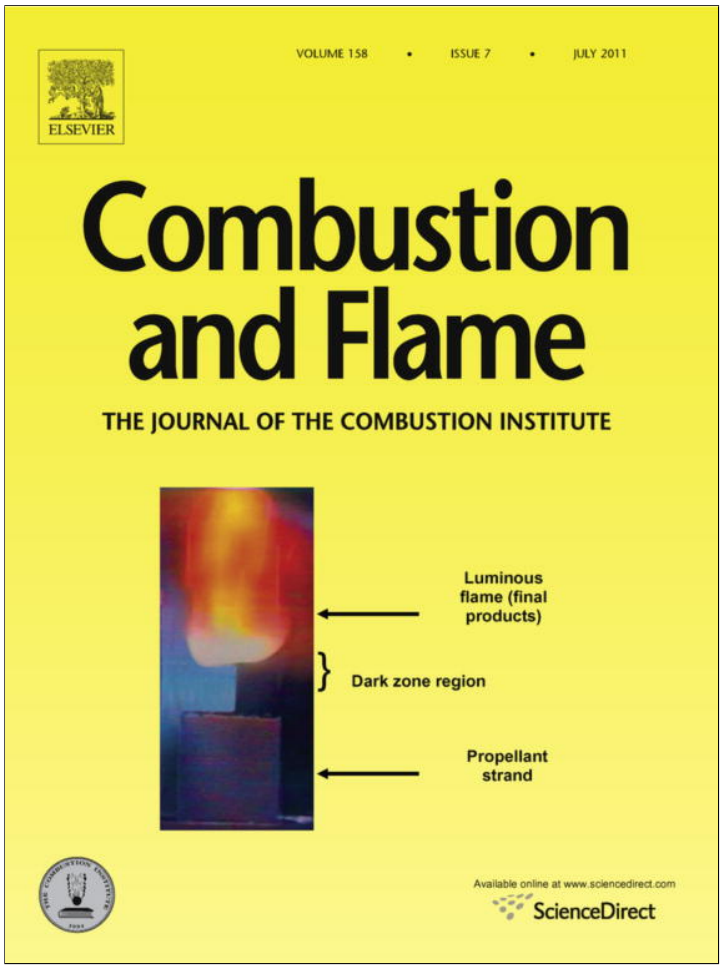

Combustion and Flame 158 (2011) 1413–1417

Contents lists available at ScienceDirect

Combustion and Flame

journal homepage: www.elsevier.com/locate/combustflame

Toward design of the pre-stressed nano- and microscale aluminum particles covered by oxide shell

Valery I. Levitas [a,*], Birce Dikici [b,1], Michelle L. Pantoya [b]

[a] Departments of Mechanical Engineering, Aerospace Engineering, and Material Science and Engineering, Iowa State University, Ames, IA 50011, USA
[b] Mechanical Engineering Department, Texas Tech University, Lubbock, TX 79409, USA

ARTICLE INFO

Article history:
Received 3 June 2010
Received in revised form 13 September 2010
Accepted 2 December 2010
Available online 22 December 2010

Keywords:
Internal stresses
Alumina shell
Flame propagation rate
Melt-dispersion mechanism

ABSTRACT

Prediction based on the recently developed melt-dispersion mechanism of reaction for nanometric (nano) and micrometer (micron) scale aluminum (Al) particles suggests a possible increase in particle reactivity if the alumina shell is pre-compressed and the Al core is pre-expanded. This prediction was checked experimentally by measuring the flame speed for Al and molybdenum trioxide (MoO_3) thermites in a semi-confined tube. Pre-stressing was produced by heating particles to several elevated temperatures, holding them at a temperature for 10 min to relax thermal stresses, and cooling them at several rates to room temperature. For the optimal thermal treatment conditions (heating to 105 °C and cooling at 0.13 °C/s), flame propagation speed increased by 31% for nanoparticles and for 41% for micron particles. Cooling at 0.06 °C/s after heating to 105 °C and cooling at 0.06 °C/s and 0.13 °C/s after heating to 170 °C either did not change the flame speed or increased it significantly less. Results are quantitatively consistent with the theoretical predictions based on the melt-dispersion mechanism.

1. Introduction

Aluminum nanoparticles are the most well-known representatives of a class of materials called nanoenergetic materials. They are being considered for overlapping technologies such as: materials synthesis application, explosive additives, and propellant rate modifiers; MEMS energy sources, as well as thermites, nanobarics, and reactive materials for ordnance applications [1,2]. Al particles are usually covered by a thin alumina (Al_2O_3) shell. For Al particles with the size greater than 20 μm and for nanoparticles at slow heating rates (less than 10^6 K/s), oxidation is controlled by diffusion of oxygen to the Al core and/or from the Al core toward the oxidizer, through a growing oxide shell [3–5]. However, for faster heating and when the initial external radius R of the Al particle reduces to 40–100 nm, reaction rates drastically increase. Flame propagation rates reach 1 km/s for loose, low density Al + MoO_3 and Al + Fe_2O_3 nano-powders in contrast to 1 m/s for micron size Al particles [6]; ignition delay times are reduced by up to three orders of magnitude [7]. To explain such drastic increase in reactivity, we recently developed new mechanochemical reaction mechanism for Al nanoparticles called the melt-dispersion mechanism [8–10]. We demonstrated that at fast heating rates the alumina shell does not fracture until the Al core melts. Aluminum melting is accompanied by a 6% volumetric expansion strain. Such a strain during fast heating produces high dynamic pressures in the range of 1–3 GPa in the molten core and tensile hoop stresses σ_h in the alumina shell that exceed the ultimate strength of alumina σ_u. This leads the dynamic fracture and spallation of the oxide shell. After shell spallation, pressure within the molten particle remains unchanged while at the bare Al surface the pressure drops down to about 10 MPa (pressure caused by surface tension and pressure of surrounding gas). Such a pressure difference causes an unloading wave that propagates to the center of the particle and creates a tensile pressure at the center of molten particle in the range of 3–8 GPa. Such a high tensile pressure exceeds the cavitation limit of liquid Al and disperses the molten Al into small bare clusters that fly at a high velocity of 100–250 m/s. Oxidation of these bare clusters is not limited by diffusion through the oxide shell, which may explain several orders of magnitude increase in reaction rate and flame speed.

Recently, this mechanism was expended to micron-scale particles in the diameter range of 1–3 μm [11,12]. Various predictions based on the melt-dispersion mechanism are confirmed experimentally [9–15]. According to the theory of elasticity, the main geometric parameter that determines stresses (and consequently fracture) in a core–shell system is the ratio of Al core radius R to shell thickness $\delta (M = R/\delta)$. All our experimental data for the relative flame speed (i.e. flame speed V normalized by the maximum possible flame speed V_{max} in the given set-up) for nanoparticles

* Corresponding author.
E-mail address: vlevitas@iastate.edu (V.I. Levitas).
[1] Current address: School of Engineering, University of North Florida, Jacksonville, FL 32224, USA.

0010-2180/$ - see front matter © 2010 The Combustion Institute. Published by Elsevier Inc. All rights reserved.
doi:10.1016/j.combustflame.2010.12.002

and micron particles with diameter of 1–3 μm are located at the single curve $V/V_{max} = f(M)$ predicted theoretically [10–12] (for fixed ultimate strength of shell and temperature of shell formation, see below). Here f is the volume fraction of melt in a particle required to fracture of the oxide shell. The melt-dispersion mechanism leads to some counterintuitive conclusions (however, confirmed experimentally) that are exactly opposite to the conclusions based on the diffusion-controlled mechanism. Thus, increase in the shell thickness (while suppressing the diffusion) promotes the melt-dispersion mechanism and increases flame speed [10]. Along the same line, complete removal of the oxide shell leads to more than order of magnitude lower flame rate [13]. The melt-dispersion mechanism also explains the effect of the heating rate [14] and compaction [15] on the flame rate.

This new mechanism leads to new parameters that control particle reactivity [9]. In this paper we will focus on the *idea of creating pre-stressed particles to increase particle reactivity* and flame speed. The idea is based on the relationship $V/V_{max} = f(M, \sigma_u, T_0)$, where the volume fraction of melt required to fracture of the oxide shell, f, is determined using the solution of an elastic problem and fracture criterion for the oxide shell; σ_u is the ultimate strength of alumina shell; and, T_0 is the temperature at which the oxide shell was formed around the Al core. During heating, the temperature increase $T - T_0$ creates thermal stresses and volume change during melting adds transformational stresses. Increasing the concentration of melt within the particle core prior to shell fracture correspondingly increases the amount of melt that will participate in the melt-dispersion mechanism and reaction. It was found [8–10] that for $M < 19$, the entire Al particle melts before oxide fracture and participates in reaction, that is why $f = 1$, $V = V_{max}$, and flame velocity reaches its maximum possible value and is independent of relative particle size M. For larger M, concentration of melt and flame velocity decrease with growing M. In this region, f and *flame speed can be increased by reducing pressure in the core and tensile stresses in the shell and delaying fracture of the shell* to higher values of f. This can be done by reducing thermal stresses due to reduction in difference $T - T_0$, i.e. by *increasing temperature at which initial oxide shell* is formed. Currently, T_0 coincides with the room temperature. However, increasing T_0 will result in tensile pressure within the core and compressive stresses in the shell at room temperature. In this way, particles were manipulated to be pre-stressed with initial stresses opposite to those that appear due to heating and melting. Systematic experimental study of the effect of pre-heating and cooling with different rates was performed in [16]. Here we will use some of experimental results from [16] combined with the theory based on the melt-dispersion mechanism [9] to prove the concept of producing pre-stressed nano and micron-scale Al particles and to demonstrate their increased flame rate.

2. Producing and testing pre-stressed aluminum particles

Since passivation of commercially available Al particles occurs at room temperature, i.e. $T_0 = T_r$, we suggest the following way to restructure of the oxide shell to change T_0. From the mechanical point of view, T_0 is the temperature at which particle is stress-free. When particles are heated to some temperature T, thermal stresses appear due to difference in thermal expansion coefficients of Al and alumina (compressive in a core and tensile in a shell) that are proportional to $T - T_0$. Holding particles for some time at temperature T_h will lead to stress relaxation due to inelastic relaxation processes in the oxide shell. Complete stress relaxation at temperature T_h effectively change temperature T_0 from $T_0 = T_r$ to $T_0 = T_h$. During cooling particles down to the room temperature, internal stresses of the opposite sign appear (i.e. tensile in a core and compressive in a shell) that are proportional to $T - T_h$. To avoid internal stress relaxation during cooling, the cooling rate must be high enough to reduce the duration particles are at elevated temperature. Thus, heating particles to and holding them at temperature T_h until complete stress relaxation following fast cooling to avoid stress relaxation results in pre-stressed particle with the stress-free temperature $T_0 = T_h$. Holding particles at elevated temperature may lead also to evaporating water and some other inclusions, healing possible damage, and removing aging effects. Stress relaxation in Al core–alumina shell system is in agreement with results in [16], stated that the change in lattice parameter of Al during heating of Al nanoparticles is almost independent of the size of particle and does not differ appreciably from that for bulk Al.

Details of experimental study are given in [17] but will be summarized here. Spherical nano- and micron-scale Al particles were studied (Table 1). Each type of Al was combined with nano-scale rod-like MoO_3. A loose powder Al–MoO_3 mixture with a density of 8% of the theoretical maximum density and an equivalence ratio of 1.2 was studied. Test conditions and results are summarized in Table 2 [17]. To characterize the mixtures, standard tests at room temperature without heat treatment were performed. It is noted that the experimentally measured flame rate for the nanoparticle mixtures is 627 m/s and lower than 950 m/s reported earlier for similar particles in a similar set-up [6,10]. Also, the flame rate of 205 m/s was also lower than 244 m/s for 1–3 μm particles reported earlier [11,12]. This difference may be related to change in passivation technology by the manufacturer. It is noted that further investigations related to the influence of passivation environment on particle reactivity are ongoing and will be reported by the authors in the near future.

After heating to 105 °C, holding for 10 min and cooling to room temperature at 0.13 °C/s (regime ↑105-10 min-↓0.13 °C/s), flame speed was significantly increased to 820 m/s for nanoparticles and 290 m/s for micron particles. At the same time, after heating to 105 °C, holding for 10 min and cooling to room temperature at 0.06 °C/s (regime ↑105-10 min-↓0.06 °C/s), flame speed practically did not change in comparison with non-heat-treated samples: it

Table 2
Summary of flame propagation results [17].

Test temperature (°C)	Regime	Flame propagation speed (m/s)	
		Micron	Nano
25		205 ± 6	627 ± 19
25	↑105-10 min-↓0.06 °C/s	223 ± 11	631 ± 32
25	↑105-10 min-↓0.13 °C/s	290 ± 6	820 ± 32
105	↑105-10 min	343 ± 3	909 ± 45
105	↑105	330 ± 17	1002 ± 60
25	↑170-10 min-↓0.06 °C/s	226 ± 7	641 ± 32
25	↑170-10 min-↓0.13 °C/s	214 ± 11	737 ± 37
170	↑170-10 min	347 ± 10	948 ± 47
170	↑170	315 ± 16	960 ± 67

Table 1
Parameters of aluminum particles.

Material	Manufacturer	Particle diameter	Oxide thickness (nm)	Relative particle diameter, M
Al-nano	NovaCentrix	80 nm	4	9
Al-micron	Alfa Aesar	3–4.5 μm	2	750–1125

was 631 m/s for nanoparticles and 223 m/s for micron particles. Thus, if a holding time of 10 min was sufficient for increasing T_0 to 105 °C and this temperature (at which system is stress-free) did not change during cooling at 0.13 °C/s due to stress relaxation, then pre-stressing indeed lead to a significant increase in flame rate. However, cooling at 0.06 °C/s was not fast enough and internal stresses relaxed, which is consistent with lack of change in the flame rate after such a heat treatment.

For comparison, Al particles were tested at 105 °C, after 10 min of holding (regime ↑105-10 min) and immediately after reaching this temperature (regime ↑105). For micron-scale particles, flame rate for both conditions was approximately the same (343 and 330 m/s, respectively). For nanoparticles, flame speed was 909 m/s with holding and 1002 m/s without holding. Increase in flame speed with increasing temperature of experiment is expected because elevated temperature increases enthalpy of reactants, adiabatic flame temperature and reduces ignition time. The reason why holding the nanoparticle mixture at 105 °C reduced flame speed in comparison with the case without holding is not clear. Elevated initial temperature may lead to shorter ignition time for particles with non-relaxed thermal stresses (without holding, T_0 = 25 °C) than with relaxed thermal stresses after holding and T_0 = 105 °C.

The same set of experiments was performed with maximum pre-heating temperature of 170 °C. The flame speed for regime ↑170-10 min-↓0.06 °C/s is practically the same as for particles without heat treatment and for the regime ↑105-10 min-↓0.06 °C/s, both for nano- and micron particles. That means that such a heat treatment does not pre-stress particles, presumably due to low cooling rate.

For the regime with higher cooling rate, ↑170-10 min-↓0.13 °C/s, flame speed for micron particles was also the same as for non-heat-treated particles and much lower than for the regime ↑105-10 min-↓0.13 °C/s with lower heating temperature and the same cooling rate. For the regime ↑170-10 min-↓0.13 °C/s, flame speed for nanoparticles was somewhat higher than for non-heat-treated particles and much lower than for the regime ↑105-10 min-↓0.13 °C/s with lower heating temperature and the same cooling rate. It looks like some undesirable processes occur at 170 °C in comparison with 105 °C.

For comparison, for the regime ↑170-10 min, flame rate for micron-scale particles is the same as for regime ↑105-10 min, while for nanoparticles it is slightly higher. At the same time, for the regime ↑170, flame rate for both nano- and micron-scale particles are slightly lower than for regime ↑105. While it is expected that increase in initial temperature of reactant will increase the flame rate, this is not the case. This also confirms that some undesirable processes occur at 170 °C. They may be related to agglomeration of particles. In future, we will try to increase cooling rate to study whether it will increase the flame speed, because at higher temperature, higher cooling rate is required to avoid stress relaxation.

3. Theoretical estimates and discussion

Pressure in the Al sphere, p, and maximum tensile hoop stresses in aluminum oxide shell at the interface with the Al sphere, σ_h, are found in [9]:

$$p = \frac{12(m^3-1)(\varepsilon_2^i-\varepsilon_1^i)G_2K_1K_2}{H} + \frac{2K_1(4G_2+3m^3K_2)\Gamma_1}{RH} + \frac{(2\Gamma_2+p_gRm)m^2K_1(4G_2+3K_2)}{RH} \quad (1)$$

$$\sigma_h = -\frac{6(m^3+2)(\varepsilon_2^i-\varepsilon_1^i)G_2K_1K_2}{H} + \frac{4(m^3+2)G_2K_2\Gamma_1}{RH} + \frac{(2\Gamma_2+p_gRm)m^2(-2G_2K_1+3(2G_2+K_1)K_2)}{RH} \quad (2)$$

where $m = 1 + 1/M$, subscript 1 is for Al and 2 is for alumina, G and K are the shear and bulk moduli, $K_1 = fK_1^m + (1-f)K_1^s$ is the bulk modulus of Al melt–solid mixture, subscripts s and m are for the solid and melt phases, p_g is the pressure of the gas, Γ_1 and Γ_2 are the surface tensions at the aluminum–alumina interface and alumina–gas interface, and $H = 3m^3K_1K_2 + 4G_2(K_1 + (m^3-1)K_2)$. Inelastic strain is give by equations

$$\varepsilon_1^i = -(\alpha_1^S(T_m - T_0) + (1-f)\alpha_1^S(T-T_m) + f\alpha_1^m(T-T_m) + f\varepsilon^m)$$
$$\varepsilon_2^i = -\alpha_2(T-T_0) \quad (3)$$

where α is the linear thermal expansion coefficients, T_0 is the temperature at which the initial oxide shell was formed on the Al particle (i.e. temperature at which internal thermal stresses are zero), and $3\varepsilon^m$ the volumetric expansion during melting of Al.

In [10], the following equation for the flame propagation rate V was derived

$$V/V_{\max} = f \quad \text{for } 0 < f \leqslant 1 \quad (4)$$

$$f = (-B + \sqrt{B^2 - 4AC})/2A \quad (5)$$

where $V_{\max}$ is the maximum velocity that can be achieved for relatively small M (Fig. 1) in the same experimental set-up, for the same mass density of the powder, and for the same oxidizer, f is the volume fraction of melt in Al core necessary to fracture of the oxide shell,

$$A = 6\delta\varepsilon^m\Delta K(2+m^3)MG_2K_2$$

$$B = \Delta km^2(\delta(1+M)p_g + 2\Gamma_2)(2G_2-3K_2) + 6\delta(2+m^3)M(\varepsilon^mK_S + \Delta\alpha\Delta K\Delta T)G_2K_2 - \delta\Delta KM(4G_2+3m^3K_2)\sigma_u$$

$$C = 6\delta(2+m^3)M\Delta\alpha K_S\Delta TG_2K_2 - 4(2+m^3)\Gamma_1G_2K_2 + m^2(\delta(1+M)p_g + 2\Gamma_2)(2K_SG_2 - 3(K_S+2G_2)K_2) - M\delta\sigma_u(3K_SK_2m^3 + 4G_2(K_s + (m^3-1)K_2))$$

In this equation, ΔK is the difference in bulk moduli between liquid and solid Al, ΔT is the difference between the melting temperature and the passivation temperature, T_0, at which the initial oxide shell was formed, σ_u is the ultimate strength of alumina, and $\Delta\alpha$ is the difference in linear thermal expansion coefficients between solid Al and alumina. All parameters in Eq. (5) can be found in [9].

Proportionality of $V/V_{\max}$ and f was obtained empirically [10,11]. Eq. (5) for f was obtained analytically from the fracture criterion for oxide shell, i.e. from the condition that the magnitude

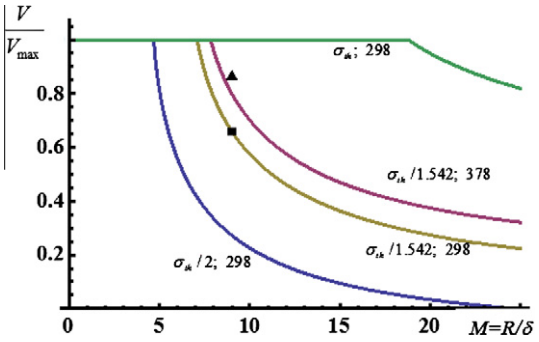

Fig. 1. Relative flame velocity $V/V_{\max}$ versus relative particle size $M = R/\delta$ for various values of the ultimate strength of the oxide shell (as fraction of σ_{th}) and passivation temperature T_0 (K), shown near the curves. Lines are calculated using Eqs. (4) and (5). Square is for the experimental value for Al nanoparticles at T_0 = 298 K, while triangle is for the experimental value at T_0 = 378 K.

of hoop stresses σ_h (Eq. (2)) reaches the ultimate strength of alumina, $-\sigma_h = \sigma_u$. Physically, Eq. (4) means that the entire molten Al which induced fracture of the oxide shell, participates in the melt-dispersion mechanism during time scales of ~10 μs (i.e., while the flame front passes through). The remaining non-dispersed Al reacts over longer time scales and does not contribute to the flame rate V. Solid lines in Fig. 1 are calculations of f versus M for $\delta = 4$ nm (f very weakly depends on δ) and several values of the ultimate strength of alumina σ_u expressed in terms of estimated value of theoretical strength $\sigma_{th} = E/30 = 11.33$ GPa, and for two values of T_0. In Fig. 1, experimental data for Al nanoparticles with $T_0 = 298$ K and $T_0 = 378$ K are superposed to the theoretical curves obtained with the help of Eqs. (4) and (5). Maximum flame velocity V_{max} is chosen to be 950 m/s, like in our previous studies [6,10], because the same set-up was used. For nanoparticles with $T_0 = 298$ K, $V/V_{max} = 0.66$, which is much below than the value 1 obtained for $M < 19$ in previous studies [11,12]. The only possible reason based on Eqs. (4) and (5) may be related to the reduced values of the ultimate strength of the shell σ_u in comparison with the theoretical strength σ_{th} used to fit experimental data in [7,8]. Ultimate strength for brittle materials has significant scatter and reduction for the nanoparticles studied here in comparison with nanoparticles studied in [8–12] may be related to change in passivation technology, e.g. using air mixture of nitrogen with oxygen rather than mixture of inert gas with oxygen. Various impurities can reduce strength of the shell. Thus, experimental value $V/V_{max} = 0.66$ for $T_0 = 298$ K and $M = 9$ can be obtained using Eqs. (4) and (5) for $\sigma_u = \sigma_{th}/1.542$. Then for the same σ_u for $T_0 = 378$ K Eqs. (4) and (5) give $V/V_{max} = 0.80$, which is close to the experimental value of 0.863. For comparison, for $T_0 = 378$ K Eqs. (4) and (5) give the experimental value $V/V_{max} = 0.863$ for $\sigma_u = \sigma_{th}/1.50$, i.e. for increase in ultimate strength just by 3%.

In Fig. 2, similar experimental and theoretical results are presented for Al micron-scale particles with the same maximum flame propagation speed $V_{max} = 950$ m/s. In the range of the experimental values of M, 750–1125, calculated relative flame rate weakly depends on M, so we chose $M = 1000$. The experimental value $V/V_{max} = 0.215$ for $T_0 = 298$ K can be obtained using Eqs. (4) and (5) for $\sigma_u = \sigma_{th}/1.261$. Then for the same σ_u for $T_0 = 378$ K Eqs. (4) and (5) give $V/V_{max} = 0.305$, which coincides with the experimental value.

Thus, our theoretical prediction that the increase of flame speed after subjecting Al nano- and micron particles by heating to 105 °C, holding for 10 min and cooling with the rate of 0.13 K/s is due to change in the temperature T_0 at which particle is stress-free from 25 °C to 105 °C, is in quantitative correspondence with experiment. There is no any evidence that such a treatment changes the ultimate strength of alumina shell.

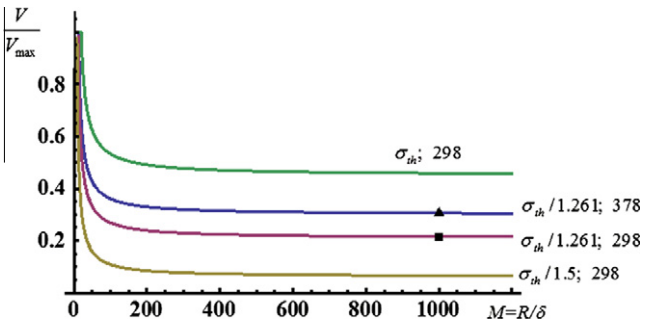

Fig. 2. Relative flame velocity V/V_{max} versus relative particle size $M = R/\delta$ for various values of the ultimate strength of the oxide shell (as fraction of σ_{th}) and passivation temperature T_0 (K), shown near the curves. Lines are calculated using Eqs. (4) and (5). Square is for the experimental value for Al micron-scale particles at $T_0 = 298$ K, while triangle is for the experimental value at $T_0 = 378$ K.

Let us estimate pressure in Al core and hoop stress in alumina shell using Eqs. (1) and (2) with volume fraction of melt $f = 0$, first for nanoparticles. For $T_0 = T = 298$ K, one has compressive pressure $p = -0.08$ GPa in Al and the compressive hoop stress $\sigma_h = -0.19$ GPa due to surface tension at the Al–alumina and alumina–gas interfaces. Heating to $T = 378$ K leads to $p = -0.20$ GPa and $\sigma_h = 0.37$ GPa, while heating to $T = 443$ K leads to $p = -0.30$ GPa and $\sigma_h = 0.82$ GPa. If we change T_0 to any current temperature, $T_0 = T$, we obtain the same stresses due to surface tension, i.e. $p = -0.08$ GPa in Al and $\sigma_h = -0.19$ GPa in alumina. Changing T_0 to 378 K induces at room temperature $p = 0.04$ GPa in Al and $\sigma_h = -0.74$ GPa in alumina.

Consequently, our optimal heat treatment added tensile pressure 0.12 GPa in Al and compressive stress 0.55 GPa in alumina. Changing T_0 to 443 K would create at room temperature $p = 0.14$ GPa in Al and $\sigma_h = -1.20$ GPa in alumina.

For micron-scale particles, for $T_0 = T = 298$ K, one obtains compressive pressure $p = -0.0021$ GPa in Al and the compressive hoop stress $\sigma_h = -0.0051$ GPa due to surface, both significantly lower than for nanoparticles. Heating to $T = 378$ K produces pressure $p = -0.0038$ GPa and hoop stress $\sigma_h = 0.865$ GPa, while heating to $T = 443$ K gives $p = -0.0052$ GPa and $\sigma_h = 1.573$ GPa. Changing T_0 to 378 K produces at room temperature $p = 0.0004$ GPa in Al and $\sigma_h = -0.876$ GPa in alumina. Consequently, our optimal heat treatment added tensile pressure 0.0017 GPa in Al and compressive stress 0.871 GPa in alumina. Since our goal is to delay fracture of oxide shell, change in hoop stress in shell is of most importance. Note that changing T_0 to 443 K would create at room temperature $p = 0.0011$ GPa in Al and $\sigma_h = -1.583$ GPa in alumina.

4. Concluding remarks

In the paper, we presented proof of concept for the design of pre-stressed Al nano- and micron size particles for energetic applications, which was predicted theoretically. It was demonstrated that flame rate can be essentially increased (by 30–40%) by special thermal treatment of the particles. Thus, to create preliminary compressive stresses in an alumina shell (and, consequently, tensile pressure in a core), particles were heated to several different temperatures, held at this temperature for 10 min to relax thermal stresses, and cooled with several rates to room temperature. Optimal (within our testing matrix) thermal treatment conditions were found, and they are the same for nano- and micron-scale particles. Experimental results are found to be quantitatively consistent with the theoretical predictions based on the melt-dispersion mechanism. This also serves as a strong confirmation for the melt-dispersion mechanism.

While the above experiments were performed for Al particles combined with a metal oxide (MoO_3), the acceleration of Al oxidation is expected for other systems that employ nanometric and micrometric Al particles, provided that the conditions for operation of the melt-dispersion mechanism are satisfied. In particular, (a) the heating rate should exceed 10^6 K/s [14]; (b) relative particle size M should not significantly exceed 1000, see Fig. 2; (c) the shell must be relatively free of imperfections such that the shell strength of alumina approaches the theoretical maximum [9,14]. If these conditions of operation for the melt-dispersion mechanism are met, then the results shown here for a thermite system should transcend to other formulations that include nano- and micron-scale Al, such as propellants, explosives and pyrotechnics. Also heat treating Al particles can enable the melt-dispersion mechanism when otherwise not applicable.

In future research, stresses in Al core will be measured using X-rays and results will be compared to theoretical predictions. Determination of stress relaxation mechanism and its temperature

dependence is of fundamental and applied interest. This mechanism also controls the melting temperature via reducing the pressure build-up in Al nanoparticles [18]. Identifying the reasons that prevent increases in particle reactivity with further increases in the temperature of the thermal treatment will allow us to reduce or eliminate them. Further progress may be obtained if the oxide shell is initially produced at high temperature rather than restructured by heat treatment.

Acknowledgments

The authors gratefully acknowledge support from the National Science Foundation under contract CBET-0755236, managed by Drs. Phillip Westmoreland and Arvind Atreya and the Office of Naval Research under contracts N00014-08-1-1262 and N00014-08-1-0104 all managed by Dr. Clifford Bedford.

References

[1] E.L. Dreizin, Prog. Energy Combust. Sci. 35 (2009) 141167.
[2] C. Rossi, K. Zhang, D. Est'eve, P. Alphonse, P. Tailhades, C. Vahlas, J. Microelectromech. Syst. 16 (4) (2007) 91931.
[3] K. Park, D. Lee, A. Rai, D. Mukherjee, M. Zachariah, J. Phys. Chem. B 109 (2005) 7290.
[4] A. Rai, K. Park, L. Zhou, M. Zachariah, Combust. Theor. Model. 10 (2006) 843.
[5] B.Z. Eapen, V.K. Hoffmann, M. Schoenitzand, E.L. Dreizin, Combust. Sci. Technol. 176 (1055–1069) (2004) 216–219.
[6] B. Bockmon, M. Pantoya, S. Son, B. Asay, J. Mang, J. Appl. Phys. 98 (2005) 064903.
[7] J. Granier, M.L. Pantoya, Combust. Flame 138 (2004) 373.
[8] V.I. Levitas, B.W. Asay, S.F. Son, M.L. Pantoya, Appl. Phys. Lett. 89 (2006) 071909.
[9] V.I. Levitas, B.W. Asay, S.F. Son, M.L. Pantoya, J. Appl. Phys. 101 (2007) 083524.
[10] V.I. Levitas, M. Pantoya, B. Dikici, Appl. Phys. Lett. 92 (2008) 011921.
[11] V.I. Levitas, M. Pantoya, K.W. Watson, Appl. Phys. Lett. 92 (2008) 201917.
[12] K.W. Watson, M.L. Pantoya, V.I. Levitas, Combust. Flame 155 (2008) 619–634.
[13] B. Dikici, M.L. Pantoya, V.I. Levitas, R.J. Jouet, Energy Fuels 23 (2009) 4231–4235.
[14] V.I. Levitas, Combust. Flame 156 (2009) 543–546.
[15] M.L. Pantoya, V.I. Levitas, J.J. Granier, J.B. Henderson, J. Propul. Power 25 (2009) 465–470.
[16] B. Rufino, M.-V. Coulet, R. Bouchet, O. Isnard, R. Denoyel, Acta Mater. 58 (2010) 4224–4232.
[17] B. Dikici, M.L. Pantoya, V.I. Levitas, Combust. Flame 157 (2010) 1581–1585.
[18] V.I. Levitas, M. Pantoya, G. Chauhan, I. Rivero, J. Phys. Chem. C 113 (2009) 14088–14096.